Korean J. Chem. Eng., 33(7), 2097-2106 (2016)
DOI: 10.1007/s11814-016-0047-0

pISSN: 0256-1115
eISSN: 1975-7220

Coupling conversion of methanol and 1-butylene to propylene on HZSM-5 molecular sieve catalysts prepared by different methods

Ting Bai, Xin Zhang†, Xiling Liu, Tengfei Chen, and Wentao Fan

School of Chemical Engineering, Northwest University, No.229, Taibai North Road, Xi'an, 710069, Shaanxi, China
(*Received 30 October 2015 • accepted 11 February 2016*)

Abstract−A series of HZSM-5 catalysts were synthesized by different methods. The physicochemical properties of the HZSM-5 catalysts were characterized by XRD, SEM, N_2 isothermal adsorption-desorption, NH_3-TPD, Py-IR and TGA, respectively. The results indicated that different preparation conditions lead to different morphologies, textures and the distribution of acid sites. The nanosized HZSM-5 catalysts exhibited better catalytic reactivity and coke capacity than the micro-sized HZSM-5 because nanosized HZSM-5 had larger specific surface area, higher pore volume, more exposed channels and more accessible acid sites. The large particles of NZ-3 in a reasonable range and the smooth surface were conducive to product diffusion; therefore, NZ-3 exhibited higher specific propylene yield and stability than the other nanosized catalysts. The moderate density and distribution of acid sites on NZ-3 also favored the formation of propylene.

Keywords: Methanol, 1-Butylene, Propylene, HZSM-5 Zeolite, Morphology, Acidity

INTRODUCTION

Propylene is an important chemical material for producing polypropylene, acrylic acid, acrylonitrile, and propylene oxides. A promising way of producing propylene by coupling conversion of methanol and C_4 hydrocarbon, which was first proposed by Nowak et al. [1], has received widespread attention in recent years. Methanol was obtained from resources alternative to oil while C_4 hydrocarbon was largely generated as by-products in refineries. The effective coupling of exothermic methanol transformation and endothermic hydrocarbon cracking will achieve thermal-neutralization. It can accelerate the production of propylene and enhance propylene yield, and also efficiently prohibit the deactivation by carbon deposition [2-5].

Until now, some work on the coupling conversion of methanol and C_4 hydrocarbon has been performed. Martin et al. [3] and Lücke et al. [6] studied the coupled transformation of methanol with different C_4 hydrocarbons, liquid hydrocarbon and crude naphtha between 600 and 700 °C. Gao et al. [7] investigated the coupled conversion of methanol and C_4 hydrocarbons over Ga/HZSM-5 catalyst at moderate temperature. Mier et al. [8,9] reported that the methanol/n-butane molar ratio of 3 induced an energy-neutral integrated process in the joint transformation of methanol and n-butane. Wang et al. [4] reported that the maximum propylene yield of 44.0% was achieved at 550 °C in the transformation of methanol and 1-butylene, which was higher than those obtained in 1-butylene cracking or MTO. Chang et al. [10] investigated the coupling transformation of n-hexane and methanol over HZSM-5, and found an improvement of n-hexane activity by bimolecular mechanism when methanol was used as co-reactant. Jiang et al. [11] introduced a two-stage moving bed reactor concept to the methanol to propylene process. The simulation results showed recycle of byproducts could increase the propylene yield to 70%. Song et al. [12] investigated the aromatization of co-feeding n-butane with methanol over Zn loaded ZSM-5/ZSM-11 zeolite catalyst and discussed the synergy between the reaction of methanol and n-butane. In addition, the effects of acidity on the reactivity of catalyst in the coupling conversion were discussed in some of the literature. Martin et al. [13] reported the weaker Brønsted acidity of iron-containing zeolites led to an increased lifetime, a higher hydrocarbon conversion and stable olefin yields. Erofeev et al. [14] emphasized that the introduction of B (III) and P (V) into ZSM-5 zeolites decreased the strength and concentration of acid sites and increased the yield of lower olefins C_2-C_4 in methanol-coupled conversion of propane and butane. Mier et al. [9] found a catalyst with high acidity and considerable acid strength (≥120 $kJ \cdot mol_{NH3}^{-1}$), such as HZSM-5 (SiO_2/Al_2O_3=30), was required for the n-butane in the joint transformation of n-butane and methanol. Gong et al. [5] found the interaction of La with hydroxyl groups adsorbed on HZSM-5 surface modified the acidity from the hydroxyl groups and obtained the propylene yield of 46.0 wt% on La/HZSM-5 with 1.5 wt% load of La in the coupling conversion of methanol and C_4 hydrocarbon.

Many studies have revealed that the morphology of zeolites has a great impact on the catalytic performance. Teng et al. [15] found that the HZSM-5 zeolite with small crystal size (0.2-0.3 μm) showed better stability in the cracking of C_4 hydrocarbons. Wu et al. [16] reported that the sheet-like SAPO-34 had longer stability and higher olefin selectivity than the cubic one. Firoozi et al. [17] observed that nano HZSM-5 had higher selectivity and stability than the micro HZSM-5. To the best of our knowledge, few studies concerning the coupling conversion over HZSM-5 zeolites with different morphol-

†To whom correspondence should be addressed.
E-mail: zhangxinzhangcn@aliyun.com

ogies have been reported so far.

In this work, a series of HZSM-5 catalysts have been synthesized by different methods. The catalytic performance of these catalysts was tested in the coupling conversion methanol and 1-butylene. In addition, the samples were characterized by powder X-ray diffraction (XRD), N_2 isothermal adsorption-desorption, scanning electron microscopy (SEM), temperature-programmed desorption of ammonia (NH_3-TPD), pyridine-adsorbed infrared spectroscopy (Py-IR) and thermal gravity analysis (TGA). Based on the obtained results, the relationship among the morphology, the acidity, and the reactivity of these catalysts was discussed.

EXPERIMENTAL METHODS

1. Materials

The chemical reagents included aluminium nitrate ($Al(NO_3)_3 \cdot 9H_2O$, Tianjin Ruijinte Chem. Co., A.R.), aluminium isopropoxide (AIP, Aladdin Chem. Co., A.R.) sodium aluminate ($NaAlO_2$, Tianjin Guangfu Chem. Co., A.R.), tetraethylorthosilicate (TEOS, Tianjin Fuchen Chem. Co., A.R.), sodium hydroxide (NaOH, Tianjin Hengxing Chem. Co., A.R.), tetrapropylammonium hydroxide (TPAOH, Aladdin Chem. Co., 25 wt%), ammonium nitrate (NH_4NO_3, Chengdu Kelong Chem. Co., A.R.), hydrofluoric acid (HF, Zhengzhou Paini Chem. Co., 40 wt%).

2. Catalyst Preparation

Preparation of NZ-1. 1.5 g of aluminium nitrate was dissolved in 37.4 g aqueous solution of tetrapropylammonium hydroxide. Then, 25 g of tetraethylorthosilicate was added to the above solution. The mixture was stirred for 48 h and then heated at 50 °C for some time in vacuum. Finally, the final solution was transferred into a Teflon-lined autoclave and crystallized under autogenic pressure at 170 °C for 48 h. After that, the solid product was separated by centrifugation, washed several times with deionized water, dried overnight at 110 °C and calcined at 550 °C for 7 h. The sample was named NZ-1.

Preparation of NZ-2. 0.75 g of aluminium isopropoxide, 18.9 g of deionized water and 19.5 g aqueous solution of tetrapropylammonium hydroxide was mixed and formed a homogeneous solution. Then, 25 g of tetraethylorthosilicate was added. The final mixture was stirred for 48 h and was heated at 40 °C for some time in vacuum. The final solution was filled into a flask with a reflux condenser. The crystallization was under atmospheric pressure at 90 °C and under stirring (150 rpm). The solid product was separated by centrifugation, washed several times, dried at 110 °C overnight and calcined at 550 °C for 5 h. The sample was named NZ-2.

Preparation of NZ-3. 0.33 g of sodium aluminate, 0.29 g of sodium hydroxide, and 6.5 g of deionized water were added to 24.4 g aqueous solution of tetrapropylammonium hydroxide. Then, 25 g tetraethylorthosilicate was added under vigorous stirring to obtain a uniform gel. Finally, the gel was transferred into a Teflon-lined autoclave and crystallized under autogenic pressure at 170 °C for

Table 1. Preparation conditions of different HZSM-5 catalysts

Catalyst	Silicon source	Aluminum source	Molar composition of gel	T/°C	P	t/h
NZ-1	TEOS	$Al(NO_3)_3 \cdot 9H_2O$	$Al_2O_3 : 60SiO_2 : 23TPAOH : 650H_2O$	170	Autogenic	48
NZ-2	TEOS	AIP	$Al_2O_3 : 60SiO_2 : 12TPAOH : 900H_2O$	90	Atmospheric	90
NZ-3	TEOS	$NaAlO_2$	$Al_2O_3 : 60SiO_2 : 1.5Na_2O : 12.5TPAOH : 575H_2O$	170	Autogenic	48
MZ	TEOS	AIP	$Al_2O_3 : 60SiO_2 : 12TPAOH : 900H_2O$	170	Autogenic	120

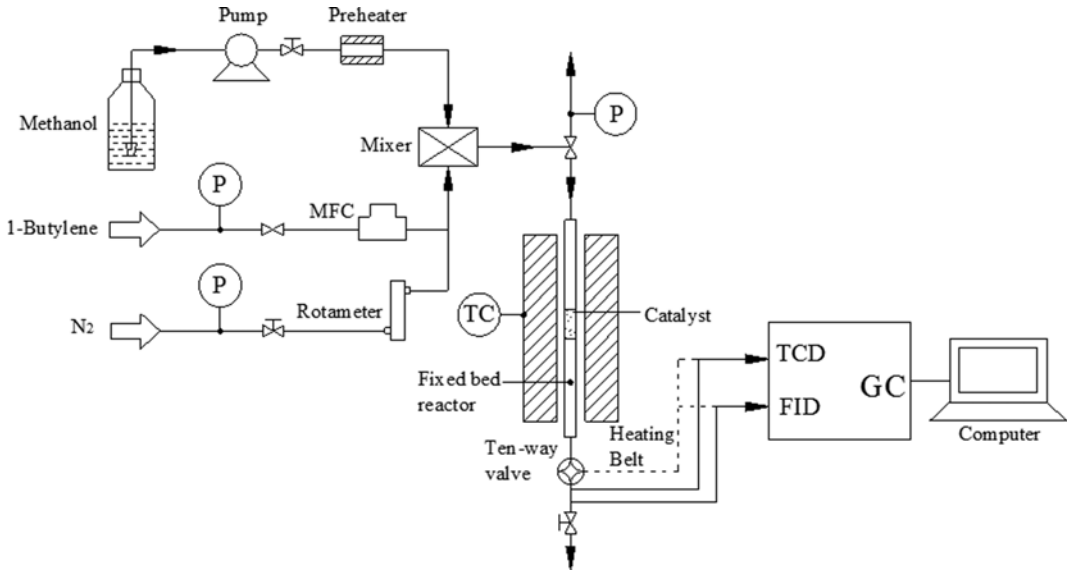

Scheme 1. Schematic diagram of catalytic reaction system for the coupling conversion of methanol and 1-butylene.

48 h. The resultant solid was separated by centrifugation, washed several times with deionized water, dried at 110 °C for 12 h, and calcined at 550 °C for 5 h. The solid powder was ion exchanged with a 1 mol/L aqueous solution of ammonium nitrate at 90 °C for 2 h. The exchanged procedure was repeated three times. The sample was washed and dried at 110 °C for 12 h, and then calcined at 500 °C for 4 h. The sample was named NZ-3.

Preparation of MZ. 0.75 g of aluminium isopropoxide, 18.9 g of deionized water, 19.5 g aqueous solution of tetrapropylammonium hydroxide and 25 g of tetraethylorthosilicate were mixed and stirred for 24 h. Then, 1.1 g of hydrofluoric acid was added to form a white gel. The gel was crystallized in a Teflon-lined autoclave at 170 °C for 120 h. The solid product was separated by filtration, washed several times, dried at 110 °C overnight and calcined at 550 °C for 5 h. The sample was named MZ. The preparation conditions for the above samples are displayed in Table 1.

3. Catalyst Test

The coupling conversion of methanol and 1-butylene was in a continuous-flow fixed-bed reactor (Scheme 1). The reactor, made of stainless steel, had an internal diameter of 10 mm and a length of 700 mm. The space up and down the catalyst bed in the reactor was filled with quartz wool. The weight of the catalyst bed was *ca.* 0.3 g and the size of the catalyst particles was *ca.* 20-40 mesh. The reaction temperature was controlled by a temperature controller (YUDIAN AI-518/518P) and measured by a K-type thermocouple. Two additional temperature controllers were used: one was to monitor the temperature distribution of the reactor, the other one was to control the transfer line temperature from the reactor outlet to the gas chromatography. Methanol (Tianjin Fuchen Chem. Co., A.R.) was injected into a preheater by a syringe pump (LabAlliance series III) and then into the mixer. 1-Butylene (Beijing Zhaoge Gas Co., 99.5 wt%) was fed directly into the mixer. The gaseous mixture of methanol, 1-butylene and N_2 passed through the catalyst bed. The off-gas was kept at 120 °C by heating belt. A small fraction of outlet gas made up of unreacted reactants and products was analyzed by GC (Ruimin Anal. GC-2060) with three analytical modules. Methane, ethylene, ethane, propylene, propane, butylenes and butane were separated by a KB-Al_2O_3/Na_2SO_4 capillary column (50 m×0.32 mm×15 μm) and detected by a flame ionization detector (FID). Benzene, Toluene, Xylene and other C_5^+ were separated by an SE-30 capillary column (30 m×0.25 mm×33 μm) and also detected by FID. Methanol was identified by a Porapak Q packed column and detected by a thermal conductivity detector (TCD). The methanol conversion and the yield of products were calculated by the following formula.

$$\text{Conversion of methanol (wt\%)} = (\text{methanol}_{in\ feed} - \text{methanol}_{in\ off\text{-}gas})/\text{methanol}_{in\ feed} \times 100\% \quad (1)$$

$$\text{Conversion of 1-butylene (wt\%)} = (\text{butylene}_{in\ feed} - \text{butylene}_{in\ off\text{-}gas})/\text{butylene}_{in\ feed} \times 100\% \quad (2)$$

$$\text{Conversion of } CH_2 \text{ (wt\%)} = n \times \text{Conversion of methanol} + (1-n) \times \text{Conversion of 1-butylene} \quad (3)$$

$$\text{Selectivity of product (wt\%)} = \text{product}/\Sigma\ \text{product} \times 100\% \quad (4)$$

$$\text{Yield of product (wt\%)} = \text{conversion of } CH_2 \times \text{selectivity of product} \times 100\% \quad (5)$$

Here, $\text{butylene}_{in\ feed}$ is the amount of 1-butylene in feed, $\text{butylene}_{in\ off\text{-}gas}$ denotes the total amount of 1-butylene, isobutylene, cis-2-butylene and trans-2-butylene in off-gas, n represents methanol/(methanol+1-butylene) molar ratio.

4. Catalyst Characterization

X-ray diffraction pattern was obtained by Rogaku Rotflex D/Max-C power X-Ray diffractometer with Cu Kα radiation (λ= 0.15046 nm) operated at 40 kV and 30 mA. The SEM experiment was on a HITACHI S-4800 instrument operating at 200 kV to observe the morphology and the particle size of the samples. N_2 adsorption-desorption characterization of the samples was at −196 °C by Micromeritics ASAP400 instrument. Prior to the adsorption, the sample was outgassed in N_2 flow at 200 °C for 3 h. The specific surface area was calculated according to BET method. Micropore volume was obtained by *t*-plot analysis of the adsorption isotherm. Mesopore volume was obtained by BJH method. The acidity of the samples was measured by temperature-programmed desorption of ammonia. The NH_3-TPD experiment was made in a continuous flow fixed-bed reactor system with thermal conductivity detector (TCD, Beifen Ruili GC-3400). Before the experiment, 0.1 g sample was placed in a quartz tube and heated at 200 °C in N_2 flow for 2 h. The sample was cooled to 50 °C and then NH_3 adsorption was performed by pulsing NH_3 to the sample until NH_3 adsorption became saturated. The catalyst was purged with 30 mL/min N_2 flow to remove NH_3 physically adsorbed on the catalyst surface. NH_3-TPD was carried out in 30 mL/min N_2 flow and from 50 to 600 °C at heating rate of 10 °C/min. Py-IR spectra were recorded by using a Bruker IF113 V FTIR spectrometer equipped with an in suit cell containing CaF_2 windows. 30 mg sample was pressed into a self-supported disk with 6.5 mm of radius and activated in an in suit cell under vacuum (1×10^{-3} Pa) at 400 °C for 2 h and then cooled to rt. Subsequently, 20 mL/min of He flow saturated with pyridine was introduced into the IR cell at rt. for 2 h to ensure that all acid sites were covered. Then the sample was, respectively, heated to 150 and 350 °C with a rate of 10 °C/min, and IR spectra were collected at the specific temperature. FTIR spectra were recorded by Nicolet FTIR 6700 spectrometer with the resolution of 4 cm^{-1}. The coke deposition measurement was performed on a Mettler TGA/SDTA851^e thermogravimetric analyzer under airflow (50 mL/min) with a heating rate of 10 °C/min from 50 to 700 °C.

RESULTS

1. Catalyst Characterization

The XRD patterns of the catalysts are given in Fig. 1. The samples exhibit the characteristic peaks of HZSM-5 ($2\theta^o$=7.8, 8.7, 22.9, 23.8, 24.2^o). This indicates that HZSM-5 framework structure could be successfully synthesized by the four methods. Compared with the MZ, the diffraction peaks of other three samples became wider. This indicates the crystal size of the three samples is smaller than that of the MZ [17,18]. In addition, the intensity of NZ-2 is lower than the other samples, which suggests it has the lowest relative crystallinity. Aguado et al. [19] reported that the crystallization of zeolite was slowed with reducing the temperature and highly crystalline samples could be obtained if the crystallization time was prolonged.

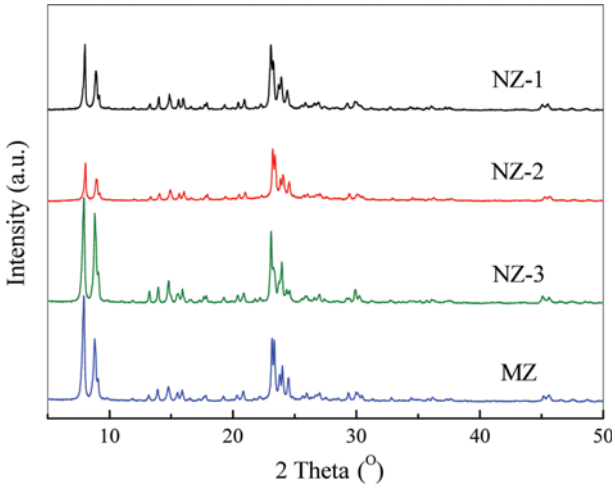

Fig. 1. XRD patterns of the catalysts.

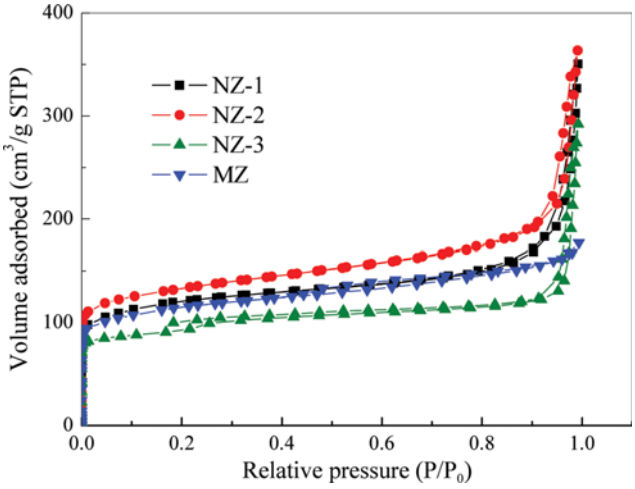

Fig. 3. N_2 adsorption-desorption isotherms of the catalysts.

Fig. 2 shows SEM images of the catalysts. The NZ-1 catalyst yielded spherical crystals in the diameter range of 20-70 nm and the particles agglomerated disorderly. NZ-2 exhibits a cauliflower-like morphology. The primary crystallites of about 30 nm agglomerated regularly and formed ellipsoids around 200 nm. This morphology is typical of the sample crystallized in clear solution at atmospheric pressure [19]. The NZ-3 sample has smooth single crystals in the size of 200 nm. In addition, MZ shows cubic-like morphology and the mean size of the crystals is around 3 μm.

Fig. 3 shows the N_2 adsorption-desorption isotherms of the catalysts. The MZ sample exhibits type I isotherm, which is characteristic of microporous material. For NZ-1, NZ-2 and NZ-3, the hysteresis loops appeared at high relative pressure (P/P_0=0.8-1.0) related to the capillary condensation in the intercrystalline pores, which was created by agglomeration of small crystals [20]. This type of isotherm is characteristic of nanoscale zeolites.

Table 2 shows the BET specific surface area (S_{BET}) and pore volume (V_{pore}) of the catalysts. The S_{BET} of NZ-1, NZ-2, NZ-3 and MZ

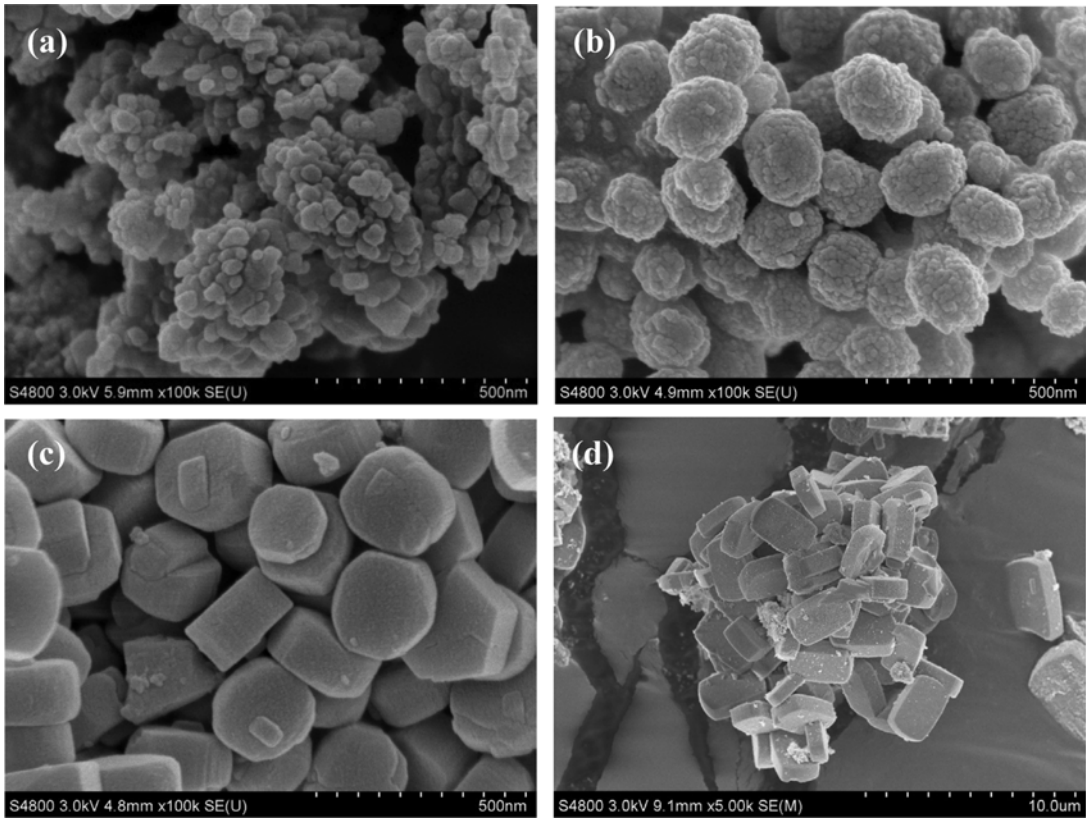

Fig. 2. SEM images of the catalysts. (a) NZ-1, (b) NZ-2, (c) NZ-3, (d) MZ.

Table 2. Texture of the catalysts

Catalyst	S_{BET} (m^2/g)	V_{pore} (cm^3/g)		
		Micro	Meso	Total
NZ-1	437	0.14	0.37	0.51
NZ-2	493	0.15	0.40	0.55
NZ-3	371	0.13	0.30	0.43
MZ	335	0.14	0.13	0.27

was 437, 493, 371 and 335 m^2/g, and the V_{pore} was 0.51, 0.55, 0.43 and 0.27 cm^3/g, respectively. Compared with MZ, the three nanoscale HZSM-5 zeolites have larger specific surface area and higher pore volume. The micropore volume of these samples is very close while their mesopore volume is significantly different. The nanosized samples have higher mesopore volume than the MZ, which is due to plenty of intercrystalline mesopores. Note that the S_{BET} of NZ-2 is considerably larger than that of the other samples. That is due to the obvious agglomeration of the primary particles in NZ-2, which is observed in Fig. 2.

The NH_3-TPD profiles are shown in Fig. 4, and the concentration and strength distribution of acid sites on the samples are summarized in Table 3. The maxima in the desorption peaks in the temperature range of 50-150, 150-350 and >350 °C are attributed to the weak, medium and strong acid sites, respectively [21]. As shown in Fig. 4, the samples present three desorption peaks (at approximately 130-140, 200-270, 380-440 °C), which indicates that

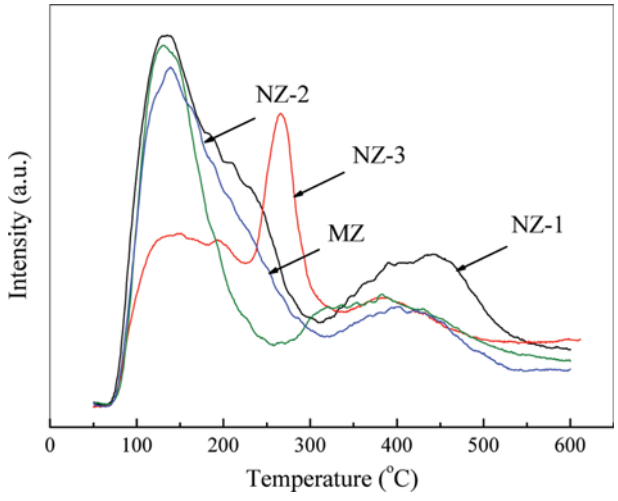

Fig. 4. NH_3-TPD profiles of the catalysts.

Table 3. Concentration and strength distribution of acid sites on the catalysts

Catalyst	Concentration of acid sites (μmol/g)			
	Weak	Medium	Strong	Total
NZ-1	43	68	55	166
NZ-2	33	45	53	131
NZ-3	58	26	45	129
MZ	41	65	37	143

weak, medium and strong acid sites exist on each catalyst. In addition, the temperature of the maximum in desorption peak indicates the acid strength [17]. Obviously, NZ-1 has the highest high-temperature desorption peak at 440 °C, which suggests the acid strength of strong acid sites on NZ-1 is higher than other samples. Zhang et al. [22] reported that only Brønsted-bound ammonia was presented when the desorption temperature was higher than 440 °C in NH_3-TPD characterization.

The NH_3-TPD profiles for the catalysts were decomposed by Gaussian fitting. And the percentage of weak, medium and strong acid sites was calculated based on the decomposition. In Table 3, the total concentration of acid sites followed the order of NZ-1> MZ>NZ-2>NZ-3, and the concentration of strong acid sites was in the descending order of NZ-1>NZ-2>NZ-3>MZ. To further analyze the types of acid sites, other methods should be performed.

The Py-IR characterization was applied to characterize the Lewis (L) and Brønsted (B) acid sites of these samples. Fig. 5 shows the Py-IR spectra of the catalysts degassed at 150 and 350 °C. The ring vibration of pyridine detected in the frequency range of 1,400-1,600 cm^{-1} is commonly used to characterize the Lewis (L) and Brønsted (B) acid sites. The band at 1,447 cm^{-1} was assigned to pyridine

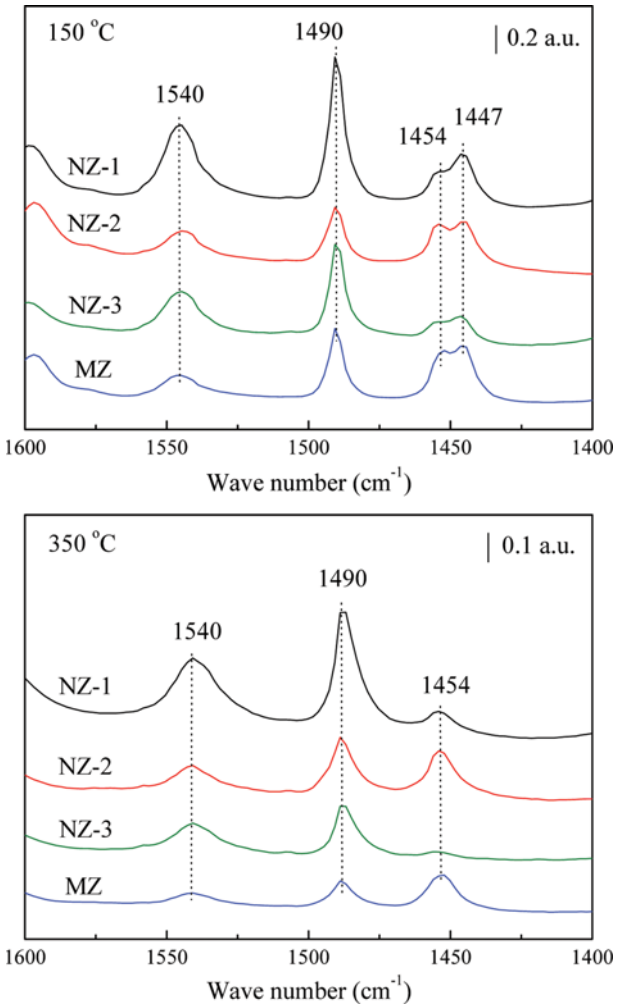

Fig. 5. Py-IR spectra of the catalysts degassed at 150 and 350 °C.

Table 4. Concentration and distribution of Brønsted and Lewis acid sites on the catalysts

Catalyst	Concentration of B (μmol/g)			Concentration of L (μmol/g)			B/L
	Weak and med.	Strong	Total	Weak and med.	Strong	Total	
NZ-1	77	64	141	31	25	56	2.52
NZ-2	42	27	69	47	34	81	0.85
NZ-3	48	35	83	37	13	50	1.66
MZ	37	16	53	80	31	111	0.48

adsorbed by hydrogen bonding, which was removed at temperature higher than 150 °C [23]. The band at 1,454 cm^{-1} corresponds to the adsorption of pyridine coordinated on Lewis acid sites [24]. The band at 1,540 cm^{-1} is due to pyridinium ions formed by the transfer of protons from Brønsted acid sites on the samples to the organic base. The band at 1,490 cm^{-1} is ascribed to the C-C stretching vibration of pyridine adsorbed on both L and B acid sites [24]. These results confirm that both B and L acid sites exist on these catalysts. The concentration of acid sites was calculated according to the method presented by Emeis [25]. On the other hand, weak and medium acid sites are defined as ones from which pyridine is removed by evacuation between 50 and 150 °C, and the strong acid sites are relative to the adsorbing pyridine after evacuation at 350 °C [5]. The concentration and distribution of L and B acid sites of the catalysts are displayed in Table 4. The concentration of total B acid sites is presented in the declining sequence of NZ-1>NZ-3>NZ-2>MZ, while the concentration of total L acid sites decreased as MZ>NZ-2>NZ-1>NZ-3. In addition, the B/L ratio follows the order of NZ-1>NZ-3>NZ-2>MZ. From the above results, we find that different preparation conditions for the HZSM-5 samples resulted in different distribution of acid sites.

Table 5. Catalytic performance of the HZSM-5 catalysts in the coupling conversion of methanol and 1-butylene

	NZ-1	NZ-2	NZ-3	MZ
Conversion (wt%)				
Methanol	100	100	100	100
1-Butylene	80.5	74.0	71.3	62.2
Selectivity (wt%)				
Methane	0.8	0.6	0.6	0.4
Ethylene	12.5	11.5	5.7	10.6
Ethane	1.5	0.2	0.2	0.8
Propylene	32.4	52.8	43.4	26.5
Propane	12.0	3.3	2.8	9.8
Butane	16.8	14.2	11.8	16.2
Benzene	0.7	1.0	1.7	1.2
Toluene	5.2	3.7	5.3	4.1
Xylene	4.8	3.9	9.0	8.6
C_5^+	13.3	8.8	19.5	21.8
Yield (wt%)				
Ethylene	10.6	9.2	4.4	7.5
Propylene	27.5	42.2	33.8	18.8
BTX	9.1	6.9	12.4	9.8

Reaction conditions: 550 °C, 0.1 MPa, space time=2.6 g_{cat}·h/mol_{CH2}, methanol/1-butylene=0.3 molar ratio, TOS=3 h

2. Catalytic Performance

The catalytic performance of the NZ-1, NZ-2, NZ-3 and MZ catalysts in the coupling conversion of methanol and 1-butylene was, respectively, tested and the results are shown in Table 5 and Figs. 6 and 7. Table 5 shows the reactivity of the HZSM-5 catalysts in the coupling conversion of methanol and 1-butylene. Under the used reaction conditions, 100 wt% of methanol conversion and distinct conversion of 1-butylene were observed on these catalysts. In addition, methane, ethylene, ethane, propylene, propane, butane, benzene, toluene, xylene and C_5^+ (all the hydrocarbons with more than five carbon atoms except for BTX (BTX included benzene, toluene and xylene)) were detected in the products. The results suggest that the coupled reaction system contains a complex series of reactions, such as dehydration, hydrocarbon cracking, hydrogen transfer, aromatization and oligomerization reaction.

From Table 5, the 1-butylene conversion follows the order of NZ-1>NZ-2>NZ-3>MZ. Meanwhile, the selectivity of propylene decreased as NZ-2>NZ-3>NZ-1>MZ, while the selectivity of ethylene declined as NZ-1>NZ-2>MZ>NZ-3. The total selectivity of BTX was in the sequence of NZ-3>MZ>NZ-1>NZ-2. Compared with the micro-sized catalyst, the three nanosized catalysts exhibited better performance for obtaining propylene in the coupling conversion of methanol and 1-butylene. The comparatively high propylene yield of 42.2 wt% was obtained on NZ-2.

Fig. 6 shows the evolution of the catalytic performance of the HZSM-5 catalysts with time on stream in the coupling conversion of methanol and 1-butylene. Methanol was almost completely converted on the four catalysts in the studied time range. From Fig. 6(a), the initial 1-butylene conversion on NZ-1 is 82.6 wt%, and then decreases to 43.7 wt% after 21 h. With increasing the reaction time, the ethylene selectivity presents a gradual decline trend. The propylene selectivity first increases, giving a maximum of 34.4 wt% at TOS=4 h, and subsequently starts to decrease. In addition, as the reaction progressed, the total selectivity of $C_{2\text{-}4}$ alkanes was falling, whereas the total selectivity of C_5^+ hydrocarbons was elevated obviously. In addition, the total selectivity of BTX on NZ-1 first increased slightly, and then reduced with the time on stream. Compared with NZ-1, the NZ-2 catalyst had lower 1-butylene conversion. However, the initial propylene selectivity of NZ-2 catalyst was 51.2 wt%, much higher than that of NZ-1, and gradually decreased to 17.4 wt% after 27 h on stream. It can be seen in Fig. 6(c), the catalytic stability of NZ-3 was superior to NZ-1 and NZ-2. At the start of the reaction, the 1-butylene conversion and propylene selectivity on NZ-3 are 76.4 wt% and 38.9 wt%, respectively. After about 30 h, they were still kept at 67.3 wt% and 36.1

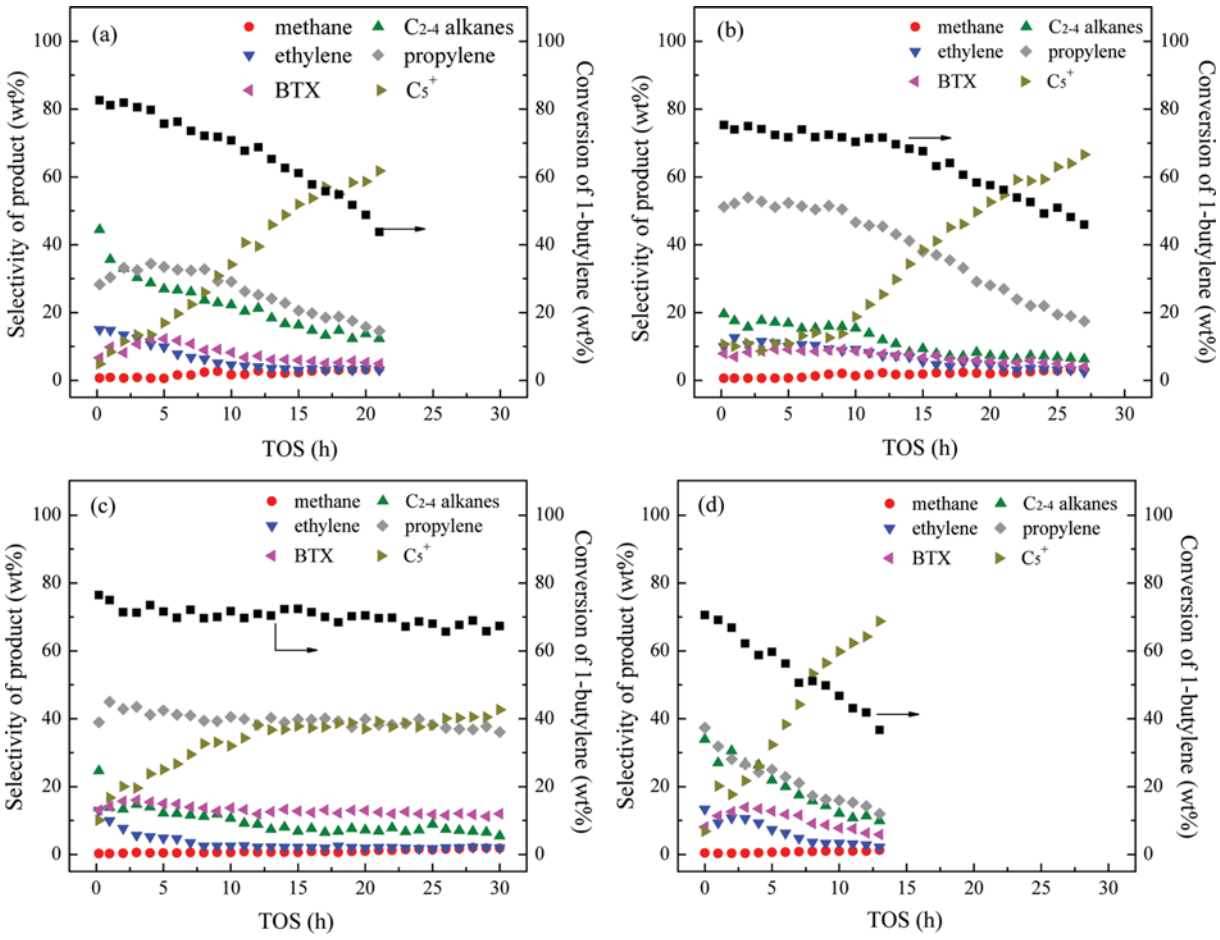

Fig. 6. Evolution of catalytic performance of the HZSM-5 catalysts with time on stream in the coupling conversion of methanol and 1-butylene. (a) NZ-1, (b) NZ-2, (c) NZ-3, (d) MZ Reaction conditions: 550 °C, 0.1 MPa, space time=2.6 g_{cat}·h/mol_{CH2}, methanol/1-butylene= 0.3 molar ratio.

wt%. Fig. 6(d) gives the change of products' distribution with time on stream on the MZ. The microsized catalyst exhibited worse stability than the above nanosized samples. The 1-butylene conversion of MZ dropped from 59.7 wt% to 36.7 wt% after only 13 h. These results confirmed that reducing the particle size of HZSM-5 zeolite could improve its catalytic performance and stability for obtaining propylene.

Fig. 7 gives the effects of reaction temperature on the catalytic performance of the samples in the reaction. Methanol was almost completely converted in the investigated reaction temperature range. From Fig. 7, when the reaction temperature increased, the 1-butylene conversion on the four samples presented a continuously increasing trend. It was reason that high temperature favored hydrocarbon cracking. It was found that the changing trend of propylene selectivity was different from that of ethylene. With the rise of reaction temperature, the ethylene selectivity monotonically increased. The propylene selectivity initially increased with the reaction temperature and reached the maximum, then started to decrease. The result implies that propylene could further transfer to secondary products by oligomerization, aromatization and coke deposition at higher reaction temperature. Therefore, in order to obtain the higher propylene yield, the proper temperature should be used in the coupling reaction.

3. The Analysis of Coke Deposited on the Used Catalysts

After the stability test, the used HZSM-5 catalysts were collected in order to analyze the coke deposition in the coupling conversion of methanol and 1-butylene. It is well known that coke is the condensation of the reaction intermediates, which was activated by the acid sites [26]. The coke amount reaches 15 wt% or even 20 wt% of catalyst and may deactivate the catalyst [27]. The TGA curves are shown in Fig. 8. The coke specific yield and the average coking rate of the used catalysts are summarized in Table 6. The weight loss below 200 °C belongs to the release of water by physical adsorption, while the weight loss between 200 and 750 °C is attributed to the combustion of coke deposited on the catalysts. The specific yield of coke (mg/m^2) is identified as the coke amount on unit-surface-area catalyst. The average coking rate is identified as the coke amount deposited on unit-surface-area catalyst in unit hour. The coke specific yield of NZ-1, NZ-2, NZ-3 and MZ is 10.2, 8.4, 14.7 and 5.4 mg/m^2, respectively. The average coking rate of NZ-1, NZ-2, NZ-3 and MZ is 0.485, 0.311, 0.263 and 0.415 mg/(m^2·h), respectively.

It is well known that coke can reduce the reactivity of catalyst by two mechanisms: active site suppression or pore blocking [28].

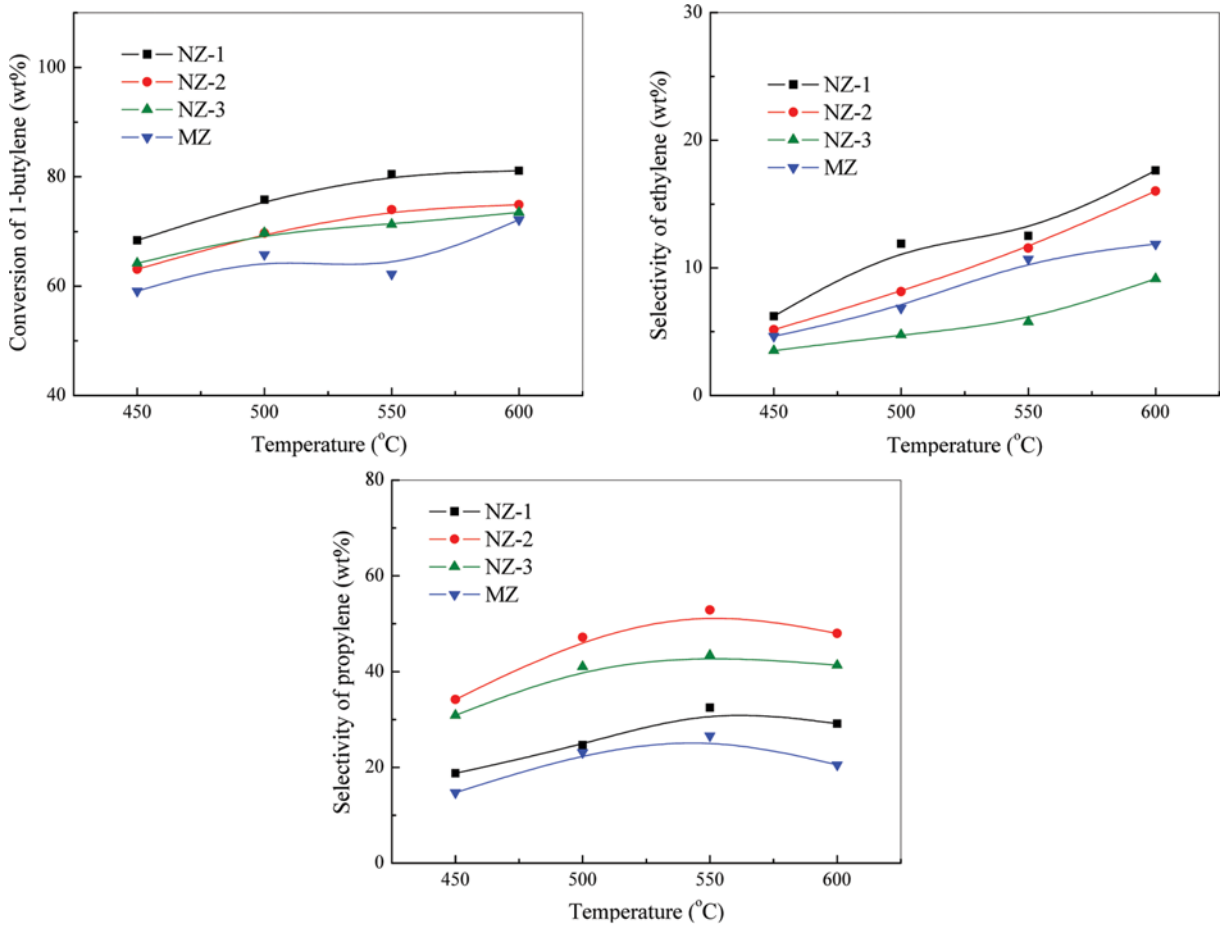

Fig. 7. Effects of reaction temperature on the catalytic performance of the HZSM-5 catalysts in the coupling conversion of methanol and 1-butylene. Reaction conditions: 550 °C, 0.1 MPa, space time=2.6 g_{cat}·h/mol_{CH2}, methanol/1-butylene=0.3 molar ratio.

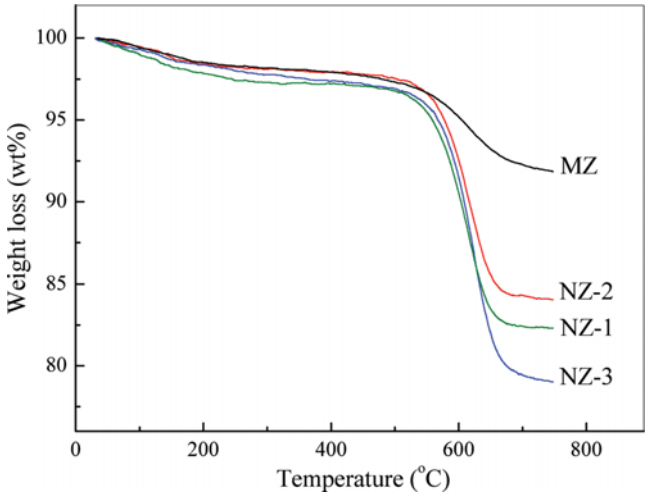

Fig. 8. TGA curves of the used HZSM-5 catalysts.

The MZ sample had a fast deactivation rate with the lowest coke content. It is deduced that the deactivation of MZ was mainly caused by blocking the pores. The reactants were prevented from diffusing into the inner channels and contacting with the internal acid sites in the MZ. Along with reducing the crystal size, the diffusion path length of the reaction medium compounds would be shorter, which means that the reaction medium compounds would be easier to diffuse from the channels of the nano-sized zeolites [15]. Therefore, the nanosized zeolites remained at higher stability than the MZ sample, even with higher coke amount. The results illustrated that the nanosized zeolites had greater coke capacity than the microsized zeolites.

Table 6. Coke specific yield and average coking rate of the used HZSM-5 catalysts

Used catalyst	Lifetime (h)	Coke specific yield (mg/m^2)	Average coking rate (mg/(m^2·h))
NZ-1	21	10.2	0.485
NZ-2	27	8.4	0.311
NZ-3	56	14.7	0.263
MZ	13	5.4	0.415

In addition, acidity is also an important factor affecting the coke behavior. For the three nanosized HZSM-5 catalysts, the average coking rate of them followed the order of NZ-1>NZ-2>NZ-3. And the total concentration of acid sites in Table 3 decreased as

NZ-1>NZ-2>NZ-3, while the strong acid sites also followed this order. The result indicates that the coking behavior on catalysts was close relative to the acidity, especially the strong acid sites. Similar results were confirmed by other researchers [29,30]. Lucas et al. [28] reported both initial coke formation velocity and final coke deposited increased when strong acidity increased.

Many works have proved the deactivation in both individual hydrocarbon cracking and MTO was fast [26,31]. By contrast, the deactivation in coupled reaction was attenuated by inhibition of polyaromatic formation due to the presence of higher olefin content in the reaction medium [2]. Moreover, the water generated from methanol dehydration could contribute to attenuating coke formation [9].

DISCUSSION

1. Relationship Among the Preparation Conditions, the Morphology of the Catalysts and the Catalytic Reactivity

In this work, a series of nano-sized HZSM-5 zeolites and a reference micro-sized sample were successfully synthesized by four different methods. The results have shown that the samples had different morphologies, acidity, textural properties, etc. These significant differences must be related to the variation of the synthesis conditions used. It has been proved that zeolite crystallization is influenced by variables during preparation, such as silica source, aluminum source, TPA^+ amount, water content, alkalinity of the reaction mixture, temperature and pressure in crystallization.

The NZ-1 was synthesized by the utilization of abundant amount of organic template under autogenous pressure. High supersaturation of the proto-nuclei was the key factor for the formation of nanocrystals [32]. Typically, nanocrystalline HZSM-5 within 20-70 nm was formed after a crystallization of 48 h. The synthesis method of NZ-2 was based on the NZ-1 process. By contrast, the crystal size of NZ-2 synthesized at low temperature under atmospheric pressure was much smaller than the crystallites of NZ-1. The use of low temperature and atmospheric pressure during the crystallization seemed to favor the nucleation step versus the crystal growth, which resulted in the formation of the partially aggregated ultrasmall nanocrystals [19]. Tosheva et al. [32] reported that low temperature favored nucleation since the activation energy needed for crystal growth was generally higher. The NZ-3 sample exhibited smooth single crystals of uniform size. The morphology might relate to the addition of Na^+ during the preparation of NZ-3, which accelerated the rate of nucleation and crystallization and favored to form crystals with well crystallinity [33].

Compared with the microsized zeolite, the nanosized sample had smaller particle size, more exposed pore mouths and more accessible acid sites [34,35]. The reaction medium products had shorter diffusion path in the nanosized zeolite. Therefore, the three nanosized HZSM-5 catalysts exhibited better reactivity and stability in the coupling conversion of methanol and 1-butylene than the MZ sample. However, we also observed both NZ-1 and NZ-2 showed worse stability than NZ-3. It was the reason that too small of the crystal and severe agglomeration went against the diffusion of products. Thus, the large particles in a reasonable range and the smooth surface were conducive to the product diffusion.

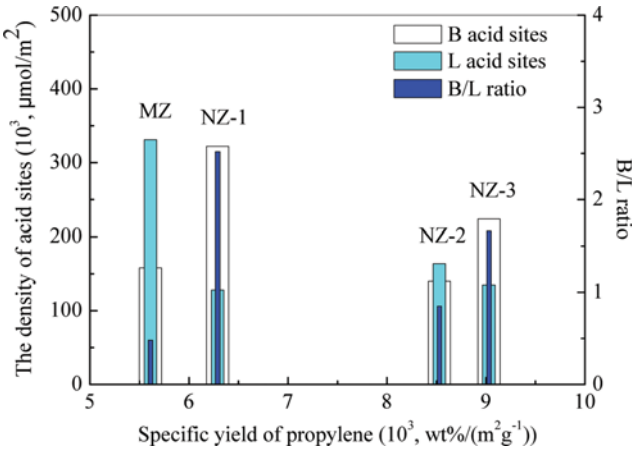

Fig. 9. Relationship of acidity and propylene yield over the HZSM-5 catalysts in the coupling conversion of methanol and 1-butylene. Reaction conditions: 550 °C, 0.1 MPa, space time= 2.6 g_{cat}·h/mol_{CH2}, methanol/1-butylene=0.3 molar ratio.

2. Effect of Acidity on the Reactivity of the Catalysts

In addition to the morphology of catalysts, the acidity also played an important role in the catalytic reactivity. To reveal the effect of acidity on the catalytic activity of the HZSM-5 zeolites, the relationship between the density of acid sites and B/L ratio with the specific yield of propylene was discussed. For comparing these samples reasonably and removing the influences of specific surface area, the propylene yield was normalized in (m^2/g), which was defined as the specific yield of propylene. The density of acid sites (μmol/m^2) is identified as the amount of acid sites on unit-surface-area catalyst. Among the four catalysts, NZ-1 showed the highest 1-butylene conversion due to its highest density of acid sites. It is known that both B and L acid sites can be used as active sites for the conversion of olefins. The increase of the acidity can enhance the conversion of olefins [36,37]. As shown in Fig. 9, the acidity had complex influences on the catalytic reactivity of HZSM-5 zeolite. In the coupled reaction of methanol and 1-butylene, the moderate density of acid sites and B/L ratio on the HZSM-5 catalyst favored the propylene formation.

It is well accepted the C_4 hydrocarbon cracking takes place by the bimolecular reaction mechanism, which involves hydride transfer, isomerization, alkylation, and β scission of carbenium ion. Light olefins are produced by oligomerization-cracking, with secondary reactions of isomerization, cyclation, aromatization, together with the coke formation. Our previous work indicated that the coupled process was conductive to butylene transformation [5]. Corma et al. [38] reported light olefins acted as active agents for cracking at high temperature. The high reaction rate for the olefins generation from methanol is effective for this activation in the coupling reaction of methanol and 1-butylene and improved the 1-butylene activity.

CONCLUSIONS

HZSM-5 was found to be a highly effective catalyst for the coupling conversion of methanol and 1-butylene. The catalytic reac-

tivity and stability of HZSM-5 catalysts in coupling conversion of methanol and 1-butylene to propylene were strongly dependent on the morphology, texture and acidity. The nanosized HZSM-5 catalysts exhibited higher propylene yield, stability and coke capacity than the microsized HZSM-5 because nanosized HZSM-5 had larger specific surface area, higher pore volume, more exposed channels and accessible acid sites. Among the investigated samples, the NZ-3 catalyst exhibited the highest specific yield of propylene, which was due to its proper density and distribution of acid sites.

A series of HZSM-5 catalysts were synthesized by different methods. The physicochemical properties of the HZSM-5 catalysts were characterized by XRD, SEM, N_2 isothemal adsorption-desorption, NH_3-TPD, Py-IR and TGA, respectively. The results indicated that different preparation conditions led to different morphologies, textures and the distribution of acid sites. The nanosized HZSM-5 catalysts exhibited better catalytic reactivity and anticoking ability than the microsized HZSM-5 because nanosized HZSM-5 had larger specific surface area, higher pore volume, more exposed channels and more accessible acid sites. The large particles of NZ-3 in a reasonable range and the smooth surface were conducive to the product diffusion; therefore, NZ-3 exhibited higher specific propylene yield and stability than the other nanosized catalysts. The moderate density and distribution of acid sites on NZ-3 also favored the formation of propylene.

ACKNOWLEDGEMENTS

We greatly acknowledge support for this work from National Ministry of Education (No. NCET-10-878), Shaanxi Province (No. 2011ZKC4-08, 2009ZDKG-70), Northwest University (10YSY08).

REFERENCES

1. S. Nowak, H. Günshel, A. Martin, K. Anders and B. Lücke, *Proceedings of the 9th International Congress on Catalysis*, Chemical Institute of Canada, Ottawa, Ontario, Canada, **4**, 1735 (1988).
2. A. T. Aguayo, A. A. Gayubo, M. Gamero, M. Olazar and J. Bilbao, *Ind. Eng. Chem. Res.*, **51**, 13073 (2012).
3. A. Martin, S. Nowak, B. Lücke and H. B. Günschel, *Appl. Catal.*, **50**, 149 (1989).
4. Z. Wang, G. Jiang, Z. Zhao, X. Feng, A. Duan and J. Liu, *Energy Fuels*, **24**, 758 (2010).
5. T. Gong, X. Zhang, T. Bai, Q. Zhang, T. Lin, M. Qi, C. Duan and L. Zhang, *Ind. Eng. Chem. Res.*, **51**, 13589 (2012).
6. B. Lücke, A. Martin, H. Günschel and S. Nowak, *Micropor. Mesopor. Mater.*, **29**, 145 (1999).
7. Z. Gao, C. Cheng, C. Tan and H. Zhu, *J. Fuel Chem. Technol.* (In Chinese), **23**, 349 (1995).
8. D. Mier, A. T. Aguayo, A. G. Gayubo, M. Olazar and J. Bilbao, *Chem. Eng. J.*, **160**, 760 (2010).
9. D. Mier, A. T. Aguayo, A. G. Gayubo, M. Olazar and J. Bilbao, *Appl. Catal. A: Gen.*, **383**, 202 (2010).
10. F. Chang, Y. Wei, X. Liu, Y. Zhao, L. Xu, Y. Sun, D. Zhang, Y. He and Z. Liu, *Appl. Catal. A: Gen.*, **328**, 163 (2007).
11. B. Jiang, X. Feng, L. Yan, Y. Jiang, Z. Liao, J. Wang and Y. Yang, *Ind. Eng. Chem. Res.*, **53**, 4623 (2014).
12. C. Song, S. Liu, X. Li, S. Xie, Z. Liu and L. Xu, *Fuel Process. Technol.*, **126**, 60 (2014).
13. A. Martin, S. Nowak and B. Lücke, *Appl. Catal.*, **57**, 203 (1990).
14. V. L. Erofeev, L. B. Shabalina, L. M. Koval and T. S. Minakova, *Russ. J. Appl. Chem.*, **75**, 752 (2002).
15. G. Teng, G. Zhao, Z. Xie and Q. Chen, *Chin. J. Catal.*, **25**, 602 (2004).
16. L. Wu, Z. Liu, L. Xia, M. Qiu, X. Liu, H. Zhu and Y. Sun, *Chin. J. Catal.*, **34**, 1348 (2013).
17. M. Firoozi, M. Baghalha and M. Asadi, *Catal. Comm.*, **10**, 1582 (2009).
18. X. Wang, X. Gao, M. Dong, H. Zhao and W. Huang. *J. Energy Chem.*, **24**, 490 (2015).
19. J. Aguado, D. P. Serrano, J. M. Escola and J. M. Rodríguez, *Micropor. Mesopor. Mater.*, **75**, 41 (2004).
20. Q. Yu, C. Cui, Q. Zhang, J. Chen, Y. Li, J. Sun, C. Li, Q. Cui, C. Yang and H. Shan, *J. Energy Chem.*, **22**, 761 (2013).
21. C. Duan, X. Zhang, R. Zhou, Y. Hua, L. Zhang and J. Chen, *Fuel Process. Technol.*, **108**, 31 (2013).
22. W. Zhang, E. C. Burckle and P. G. Smirniotis, *Micropor. Mesopor. Mater.*, **33**, 173 (1999).
23. Q. Xin and M. Luo, *Research Methods for Modern Catalysis*, Sci. Press, Beijing (2004).
24. X. Zhang, J. Zhong, J. Wang, L. Zhang and J. Gao, *Micropor. Mesopor. Mater.*, **108**, 13 (2008).
25. C. A. Emeis, *J. Catal.*, **141**, 347 (1993).
26. E. Epelde, M. Ibañez, A. T. Aguayo, A. G. Gayubo, J. Bilbao and P. Castaño, *Micropor. Mesopor. Mater.*, **195**, 284 (2014).
27. S. Aghamohammadi and M. Haghighi, *Chem. Eng. J.*, **264**, 359 (2015).
28. A. de Lucas, P. Canizares, A. Durán and A. Carrero, *Appl. Catal. A: Gen.*, **156**, 299 (1997).
29. M. Guisnet and P. Magnoux, *Appl. Catal.*, **54**, 1 (1989).
30. L. Sun, X. S. Wang, J. C. Li, A. Ma and H. C. Guo, *Reac. Kinet. Mech. Catal.*, **102**, 235 (2011).
31. G. Qi, Z. Xie, W. Yang, S. Zhong, H. Liu, C. Zhang and Q. Chen, *Fuel Process. Technol.*, **88**, 437 (2007).
32. L. Tosheva and V. P. Valtchev, *Chem. Mater.*, **17**, 2494 (2005).
33. S. D. Kim, S. H. Noh, J. W. Park and W. J. Kim, *Micropor. Mesopor. Mater.*, **92**, 181 (2006).
34. P. Zhang, X. Guo, H. Guo and X. Wang, *J. Mol. Catal. A: Chem.*, **261**, 139 (2007).
35. D. P. Serrano, R. V. Grieken, J. A. Melero, A. García and C. Vargas, *J. Mol. Catal. A: Chem.*, **318**, 68 (2010).
36. K. Tanabe, M. Misono, Y. Ono and H. Hattori, *New Solid Acids and Bases their Catalytic Properties*, Kodausha, Tokyo (1989).
37. Y. V. Kissin, *Catal. Rev.*, **43**, 85 (2001).
38. A. Corma and A. V. Orchillés, *Micropor. Mesopor. Mater.*, **35-36**, 21 (2000).